Energy deposition in thin films calculated using electron transport theory

Theodore Biewer and Peter Rez
Department of Physics and Center for Solid State Science, Arizona State University, Tempe, Arizona 85287-1504

(Received 11 April 1994; accepted for publication 24 August 1994)

In scanning electron microscopy and low voltage point-projection microscopy there is considerable interest in estimating beam damage which can be related to the energy deposited in the specimen. We derive an expression for the energy deposition using the electron transport equation and give results for beam energies of 1–10 kV incident on 100 and 200 nm carbon films. The elastic scattering was modeled using a Rutherford cross section and the inelastic scattering cross section was derived from the Bethe stopping power equation. For the 100-nm-thick amorphous carbon film 90% of the incident beam energy is deposited in the sample at 2 keV, but at 6 keV only 20% of the energy is deposited. The 200 nm sample exhibited a similar curve with 20% deposition occurring at 9 keV. Our calculations show the same variation with beam energy as reported experimental results.

An electron beam striking a specimen interacts in a variety of ways to generate signals that can give information about the composition of the specimen. For thick samples most of the beam energy is deposited in the sample, which can lead to radiation damage. Radiation damage limits the applicability of electron microscopy to sensitive biological specimens, and there is therefore great interest in finding experimental conditions that minimize damage. By contrast, in the electronics industry beam damage is used in lithography to define micron-sized areas in the production of devices. The interaction of a low energy beam with a thin specimen is also of great interest for new developments in electron microscopy, particularly the point-projection microscope.[1,2]

Electron interactions in scanning microscope specimens have been modeled using various simplified theories,[3–5] Monte Carlo methods[6–10] and the Boltzman transport equation.[11–14] An extensive review of many of these approaches has been given in the book by Reimer.[15] The advantage of the transport equation method is that the explicit analytic variation on various parameters can be explored. The most serious deficiency of the transport equation is that it can only be easily applied to simple slablike sample geometries.

The energy deposition in an infinite medium was first calculated by Spencer[16] who solved the transport equation using moments. Fathers and Rez[13] also published a calculation of the energy deposition as a function of depth in a semi-infinite slab of copper for 30 kV electrons. The results were compared with the earlier work of Spencer. More recently Valkealahti *et al.*[17] published Monte Carlo calculations of the depth distribution of energy deposition in a semi-infinite medium for silicon, aluminum, and some light element gases for electron energies between 1 and 10 kV. We use the formalism of Fathers and Rez[12,13] to derive expressions for the energy deposited in a solid film. This energy is the difference between the incident energy and that carried away by backscattered and transmitted electrons. Numerical solutions show that for thick films where the transmitted fraction is low, up to 90% of the energy of the incident beam is deposited in the sample.

In the geometry of scanning electron microscope the transport equation can be written as

$$\cos\theta\,\frac{dI(z,\theta,E)}{dz} = \int\int [\sigma(\theta,E;\theta',E')I(z,\theta',E') - \sigma(\theta',E';\theta,E)I(z,\theta,E)]\sin\theta'\,d\theta'\,dE', \tag{1}$$

where $I(z,\theta,E)$ is the flux per unit angle, per unit energy range, $\sigma(\theta,E,\theta',E')$ is the cross section for scattering of an electron at energy E, traveling in a direction specified by θ to a state in which the energy is E' and the direction θ'. The flux $I(z,\theta,E)$ can be defined in terms of $f(z,\theta,E)$, the probability of finding an electron at energy E traveling in a direction specified by θ,

$$I(z,\theta,E)=vf(z,\theta,E), \tag{2}$$

where v is the electron velocity. The flux is therefore a measure of the number of electrons crossing unit area per second with energy between E and $E-\Delta E$ and traveling at angles within a range $\Delta\theta$ of θ. Following Fathers and Rez[12,13] the transport equation can then be converted to a matrix formalism by making the angle and energy discrete variables (see also Fig. 1)

$$\cos\theta_i\,\frac{dI(z,\theta_i,E_m)}{dz} = \sum_{nj} [\sigma(\theta_i,E_m;\theta_j,E_n)I(z,\theta_j,E_n) - \sigma(\theta_j,E_n;\theta_i,E_m)I(z,\theta_i,E_m)]\sin\theta_j\,d\theta_j\,dE_n. \tag{3}$$

Convergence can be achieved with 20 angle segments covering 180° and 10 energy steps. Equation (3) can be written

 0021-8979/94/76(11)/7636/3/$6.00

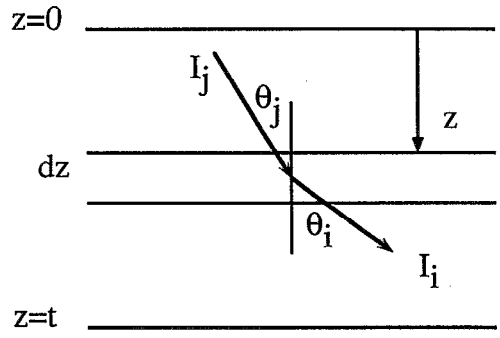

FIG. 1. Schematic diagram showing specimen and coordinate system.

with the matrix in block form where $(\mathbf{I}_0,\mathbf{I},...)$ are vectors representing groupings of the flux for the full range of polar angles at a given energy,

$$\frac{d}{dz}\begin{pmatrix}\mathbf{I}_0\\ \mathbf{I}_1\\ \mathbf{I}_2\\ \cdot\end{pmatrix}=\begin{pmatrix}\mathbf{A}^{00} & 0 & 0 & 0\\ \mathbf{A}^{10} & \mathbf{A}^{11} & 0 & \cdot\\ 0 & \mathbf{A}^{21} & \mathbf{A}^{22} & \cdot\\ \cdot & 0 & \cdot & \cdot\end{pmatrix}\begin{pmatrix}\mathbf{I}_0\\ \mathbf{I}_1\\ \mathbf{I}_2\\ \cdot\end{pmatrix}, \tag{4}$$

assuming electrons can only lose energy to the next lowest energy level. The diagonal terms represent elastic scattering, while the subdiagonal elements represent inelastic scattering. If all elements of the flux are expressed as one vector, **I**, with $n\times m$ elements where m is the number of angle segments in 180° and n is the number of energy segments, Eq. (4) can be restated as

$$\frac{d\mathbf{I}}{dz}=\mathbf{A}\mathbf{I}, \tag{5}$$

where A is the general scattering supermatrix and the solution can be written as

$$\mathbf{I}(z)=\exp(\mathbf{A}z)\mathbf{I}(0)=\mathbf{V}\exp(\Lambda z)\mathbf{V}^{-1}\mathbf{I}(0). \tag{6}$$

Here V and Λ are the eigenvectors and eigenvalues of the matrix, A. I and A can be partitioned into forward and backward scattered components, thus giving

$$\begin{pmatrix}\mathbf{I}_F(z)\\ \mathbf{I}_B(z)\end{pmatrix}=\begin{pmatrix}\mathbf{V}_1 & \mathbf{V}_2\\ \mathbf{V}_2 & \mathbf{V}_1\end{pmatrix}\begin{pmatrix}e^{\lambda z} & 0\\ 0 & e^{-\lambda z}\end{pmatrix}\begin{pmatrix}\mathbf{V}_1 & \mathbf{V}_2\\ \mathbf{V}_2 & \mathbf{V}_1\end{pmatrix}^{-1}\begin{pmatrix}\mathbf{I}_F(0)\\ \mathbf{I}_B(0)\end{pmatrix}. \tag{7}$$

Different problems can be treated by applying different boundary conditions to Eq. (7). For example, the boundary conditions for a film of thickness t are

$$\mathbf{I}_F(0)=\mathbf{I}_0$$

and

$$\mathbf{I}_B(0)=0. \tag{8}$$

After some algebra the forward and backward scattered fluxes, I, at depth z, in a film of thickness t can be written as

$$\begin{aligned}\mathbf{I}_F(z,t)=&[(\mathbf{V}_2\exp(-\lambda z)\mathbf{V}_2^{-1}-\mathbf{V}_1\exp[-\lambda(t-z)]\mathbf{V}_2^{-1}\mathbf{V}_1\\ &\times\exp(-\lambda t)\mathbf{V}_2^{-1})(1-\mathbf{V}_1\exp(-\lambda t)\mathbf{V}_2^{-1}\mathbf{V}_1\\ &\times\exp(-\lambda t)\mathbf{V}_2^{-1})^{-1}]\,I_0,\end{aligned}$$

$$\begin{aligned}\mathbf{I}_B(z,t)=&[(\mathbf{V}_1\exp(-\lambda z)\mathbf{V}_2^{-1}-\mathbf{V}_2\exp[-\lambda(t-z)]\mathbf{V}_2^{-1}\mathbf{V}_1\\ &\times(-\lambda t)\mathbf{V}_2^{-1})(1-\mathbf{V}_1\exp(-\lambda t)\mathbf{V}_2^{-1}\mathbf{V}_1\\ &\times\exp(-\lambda t)\mathbf{V}_2^{-1})^{-1}]\,I_0.\end{aligned} \tag{9}$$

The energy deposited in the film is given by the expression

$$E_D=\sum_j (I_F(E_j,0)-I_F(E_j,t)-I_B(E_j,0))E_j. \tag{10}$$

The transport equation model explicitly assumes that the solid is amorphous and that diffraction effects from coherent elastic scattering can be neglected. Following Fathers and Rez[12,13] we use a screened Rutherford cross section for the elastic scattering and derive an inelastic scattering cross section from the Bethe stopping power[18]

$$\sigma(\theta_i,E_{n-1};\theta_i,E_n)\Delta E\approx\frac{dE}{ds}\left(\frac{E_n+E_{n-1}}{2}\right). \tag{11}$$

The cross sections used in our calculations can be justified because they give excellent agreement with experimental electron backscattering yields and energy distributions as well as Monte Carlo results for normal scanning electron microscopy energies of 20–30 kV.[12,13]

There are improvements to the cross sections which could have been implemented for lower energies. In the elastic scattering cross section, the Rutherford cross section can be replaced, rather, by a cross section of the form

$$\frac{16}{a_0^2}\frac{(Z-f_x(\Delta k))^2}{(\Delta k)^4}, \tag{12}$$

where f_x is the x-ray scattering factor, a_0 is the Bohr radius, and Δk is the change in wave vector due to scattering. The inelastic scattering cross section can be taken directly from the measured energy loss spectra, appropriately scaled for beam energy. Moreover, for electrons with energy below 1 keV there is the problem of electron exchange, which has to be considered in the cross sections. Additionally, electrons at energies below 300 eV are below the ionization threshold for inner shell excitations. This might not be as serious a problem as one might suppose, since most of the contribution to stopping power, i.e. the energy deposited per atom per path length, comes from deep valence excitations with ionization energies less than 100 eV.[19]

Figure 2 shows the energy deposited in 100- and 200-nm-thick carbon films as a function of the normally incident beam energy. Calculations with 16 angle segments in 180° and 8 energy segments showed negligible differences from results calculated with 20 angle segments and 10 energy steps, indicating that the calculations have converged. These results have the same functional form as shown by Howie for a 23-nm-thick film of coronene, a carbon-based compound.[20] Figure 3 shows the percentage of beam energy backscattered and forward scattered from the sample. It is clear that when the beam energy is large the majority of the electrons pass through the thin film, as is expected. By our definition of the energy deposited in the film, Eq. (10), this implies that most of the electrons are forward scattered at small angles. Multiple large angle scattering would lead to longer path lengths

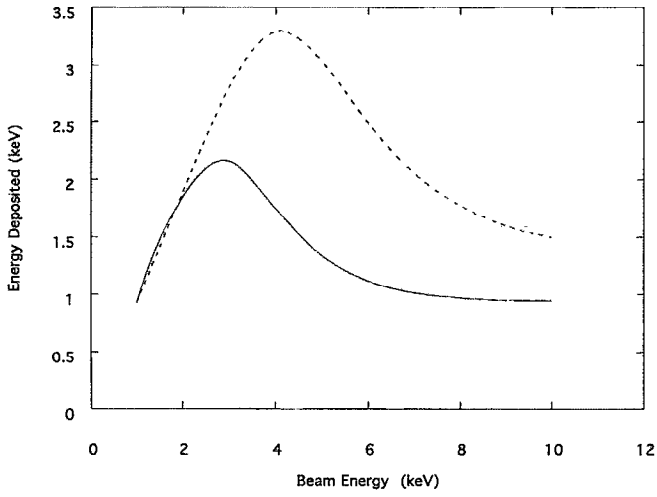

FIG. 2. Energy deposited E_D in 100-nm- (—) and 200-nm- (---) thick amorphous carbon films as a function of the incident beam energy E_0.

which means that more energy would be lost to the sample. Here we see that the fraction of energy deposited in the film goes to zero quite rapidly.

More interesting however is the low energy, 1–4 keV region in which a substantial fraction of the beam energy is imparted to the film. While the fraction of electrons backscattered is small (<15%) over the 1–10 keV region, the fraction of forward scattered electrons increases dramatically above 2 keV for the 100 nm case, and above 4 keV for the 200 nm case. In the low energy limit the sample is in effect a bulk sample and backscattering then limits the energy deposited.

Perhaps the most important implication from these results is that for samples with thicknesses of the 100–200 nm order, an electron beam of less than 3 or 4 keV will produce

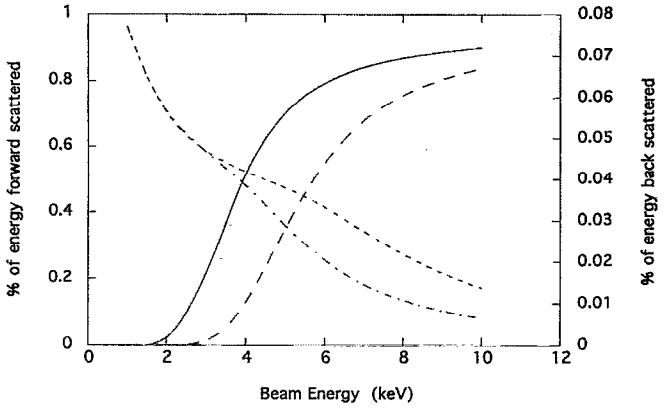

FIG. 3. As a function of the incident beam energy the left-hand scale shows the percentage of energy forward scattered from 100 nm (—) and 200 nm (– – –) amorphous carbon films. The right-hand scale shoes the percentage of energy backscattered from 100 nm (– – –) and 200 nm (---) amorphous carbon films.

substantial energy deposition. This has serious consequences for low energy electron microscopes that wish to avoid heavy sample damage. Thinner samples should allow for the use of electron beams without substantial energy deposition down to the 3 or 4 keV energy range.

We have found that at very low energies (on the order of 1–2 keV) 100- and 200-nm-thick amorphous carbon films behave very much like bulk samples. At these energies most of the incident beam energy is deposited in the sample. For the 100 nm sample as much as 90% of the beam energy is deposited. When the beam energy is increased above 2 keV the energy deposited drops off dramatically with 55% of the beam being transmitted at 4 keV. By 10 keV over 90% of the beam is transmitted. For the 200 nm sample 90% of the incident energy is deposited at 2 keV. At 6 keV the energy deposited has dropped to 45% and by 10 keV only 16% is deposited while 85% of the beam energy is transmitted through the sample. Though the data are from a much thinner sample, we produce the same functional form as the experiment. Both our results and those of Howie[20] indicate that below a certain energy a substantial amount of the beam energy is deposited in the sample. The increase in the fraction of backscattered electrons shows that a thin film behaves as a bulk sample at low energies.

It is important to note that we have modeled a simple thin film. Of interest is the condition of a thin film on a substrate, which is more relevant to layers on a semiconductor substrate. It would be worthwhile to extend the formalism to deal with this case and multilayer films.

We would like to acknowledge use of computer facilities at the National Center for High Resolution Electron Microscopy, funded by the National Science Foundation as Grant No. DMR 91-15680.

[1] J. C. H. Spence, W. Qian, and A. J. Melmed, Ultramicroscopy **52**, 573 (1993).
[2] H. J. Kreuzer, K. Nakamura, A. Wierzbicki, H. W. Fink, and H. Schmid, Ultramicroscopy **45**, 381 (1992).
[3] G. D. Archard, J. Appl. Phys. **32**, 1505 (1961).
[4] T. E. Everhart, J. Appl. Phys. **31**, 1483 (1960).
[5] K. Kanaya, S. Ono, and F. Ishigaki, J. Phys. D **11**, 2425 (1978).
[6] D. C. Joy, J. Microsc. **147**, 51 (1987).
[7] A. J. Antolak and J. Williamson W., J. Appl. Phys. **58**, 526 (1985).
[8] M. J. Berger and S. M. Seltzer, Phys. Rev. C **2**, 621 (1970).
[9] K. Murata, J. Appl. Phys. **45**, 4110 (1974).
[10] R. Shimizu, T. Ikuta, and K. Murata, J. Appl. Phys. **43**, 4233 (1972).
[11] D. B. Brown, D. B. Wittry, and D. F. Kyser, J. Appl. Phys. **40**, 1627 (1969).
[12] D. J. Fathers and P. Rez, in *Scanning Electron Microscopy*, edited by O. Johari (SEM, O'Hare, IL, 1979), p. 55.
[13] D. J. Fathers and P. Rez, in *Electron Beam Interactions with Solids*, edited by D. F. Kyser, H. Niedrig, D. E. Newbury, and R. Shimizu (SEM, O'Hare, IL, 1984), p. 193.
[14] H. Lanteri, R. Bindi, and P. Rostaing, Scan. Microsc. **2**, 1927 (1988).
[15] L. Reimer, *Scanning Electron Microscopy* (Springer, New York, 1985).
[16] L. V. Spencer, Phys. Rev. **98**, 1597 (1955).
[17] S. Valkealahti, J. Schou, and R. M. Nieminen, J. Appl. Phys. **65**, 2258 (1989).
[18] R. F. Dashen, Phys. Rev. **134**, A1025 (1964).
[19] A. Howie and F. J. Rocca, Philos. Mag. B **52**, 751 (1985).
[20] A. Howie, M. N. Mohd Muhid, F. J. Rocca, and U. Valdre, in *EMAG 87* (Institute of Physics, London, 1987), p. 155.